



Citation for published version:

Almar, R, Blenkinsopp, C, Almeida, LP, Catalán, PA, Bergsma, E, Cienfuegos, R & Viet, NT 2019, 'A new remote predictor of wave reflection based on runup asymmetry', *Estuarine, Coastal and Shelf Science*, vol. 217, pp. 1-8. <https://doi.org/10.1016/j.ecss.2018.10.018>

DOI:

[10.1016/j.ecss.2018.10.018](https://doi.org/10.1016/j.ecss.2018.10.018)

Publication date:

2019

Document Version

Peer reviewed version

[Link to publication](#)

Publisher Rights

CC BY-NC-ND

University of Bath

Alternative formats

If you require this document in an alternative format, please contact:
openaccess@bath.ac.uk

General rights

Copyright and moral rights for the publications made accessible in the public portal are retained by the authors and/or other copyright owners and it is a condition of accessing publications that users recognise and abide by the legal requirements associated with these rights.

Take down policy

If you believe that this document breaches copyright please contact us providing details, and we will remove access to the work immediately and investigate your claim.

A new remote predictor of wave reflection based on runup asymmetry

Rafael Almar¹, Chris Blenkinsopp², Luis Pedro Almeida³, Patricio A. Catalán^{4,7,8}, Erwin Bergsma^{1,3},
Rodrigo Cienfuegos^{5,7} and Nguyen Trung Viet⁶

Abstract

Reflected waves account for a significant part of the nearshore energy budget and influence incoming waves, nearshore circulation and sediment transport. The use of swash parameters to estimate wave reflection is investigated at three different beaches ranging from highly reflective to dissipative. It is observed that it is essential to account for swash processes when estimating reflection, in particular at intermediate and reflective beaches with a steep beachface. Our results show that runup asymmetry in uprush/backwash can be used as a proxy for dissipation in the swash zone: larger asymmetry values indicating greater dissipation. In our dataset, a reflection predictor based on runup asymmetry has better skill in comparison to empirical predictors based on surf similarity, because runup is a process that integrates both surf and swash zone wave transformation. Runup asymmetry behaves as a swash similarity parameter and reflects an equilibrium between swash period, slope and dissipation.

Keywords: Nearshore; video imagery; runup asymmetry; swash dissipation; reflection

Highlights:

- Link between swash parameters and wave reflection investigated at three different beaches
- Asymmetry in uprush/backwash can be considered a proxy for swash dissipation
- Evidence of equilibrium between runup asymmetry, period and slope

¹ IRD-LEGOS, Toulouse, France

² Water, Environment and Infrastructure Resilience Research Unit, University of Bath, Bath, UK

³ CNES-LEGOS, Toulouse, France

⁴ Dpt Obras civiles-Universidad Tecnica Federico Santa Maria, Valparaiso, Chile

⁵ DIHA-Pontificia Universidad Catolica de Chile, Santiago, Chile

⁶ Thuyloi University, Vietnam, Hanoi, Vietnam

⁷ Centro Nacional de Investigación para la Gestión Integrada de Desastres Naturales, CONICYT/FONDAP/1511007, Santiago, Chile

⁸ CCTVal-Centro Científico Tecnológico de Valparaíso, Valparaíso, Chile.

23

24 1. Introduction

25 Field and laboratory studies have demonstrated that incident wave energy is not entirely
26 dissipated when it reaches the shoreline. Part of the incident wave energy is reflected into deeper
27 water (Mansard & Funke, 1980; Miche, 1951; Tatavarti, Huntley, & Bowen, 1988). As a rule-of-thumb:
28 the steeper the beach, the more incident wave energy is reflected, and vice versa. At the steepest
29 beaches and in the case of long period waves, observations show that up to 60-80% of the incoming
30 wave energy is reflected (Battjes, 1974; Elgar et al., 1994). Reflected waves can strongly influence
31 and interact with incident waves; change individual wave shape (Abdelrahman and Thornton, 1987;
32 Rocha et al., 2017), intensify undertow (Martins et al., 2017), and generate standing or even resonant
33 waves (Almar et al., 2012; 2016). This effect on the hydrodynamics is thought to have a feedback on
34 submerged morphological bed forms (e.g. O'Hare and Davies, 1993; Hancock and Mei, 2008), and can
35 also modify offshore wave conditions. In deep water up to 15% of the total wave energy can be linked
36 to coastal reflection (Ardhuin and Roland, 2012) as reported in the Gulf of Guinea, West Africa (Laibi
37 et al., 2014), where beaches are generally steep and incident waves are long. Hence, it is crucial to
38 understand and accurately predict reflection at natural beaches.

39 Based on the laboratory study of Iribarren and Nogales (1949), Battjes (1974) demonstrated that
40 wave reflection is proportional to a "surf similarity" parameter ξ which quantifies surf zone
41 conditions:

42

$$43 \quad \xi = \frac{\tan(\alpha_f)}{\sqrt{H/L_0}} \quad (\text{Eq. 1})$$

44 where α_f is the foreshore slope, and H and L_0 are the wave height and deep-water wavelength
45 respectively. Dissipative conditions are generally associated with low values of ξ , typically less than
46 0.3 (Stockdon et al., 2006; Ruggiero et al., 2001; Ruessink et al., 1998, Raubenheimer and Guza, 1996;
47 Raubenheimer et al., 1995; Guza and Thornton, 1982), whereas intermediate and reflective
48 conditions are associated with larger values (Holland and Holman, 1999; Holland, 1995; Holman,
49 1986; Holman and Sallenger, 1985). The surf similarity equation provides satisfactory reflection
50 estimates for gentle slopes (low ξ) when dissipation is dominated by wave breaking, but
51 overestimates reflection for $\xi > 2.5$, when wave energy dissipation in the swash zone becomes more
52 significant (Ahrens, 1979; Seelig and Ahrens, 1981; Sutherland and O'Donoghue, 1998; Baldock, P.
53 Holmes, 1999). Furthermore, the surf similarity parameter is a seemingly weak proxy for reflection
54 in the case of complex bathymetries such as two-slope profiles (Mizuguchi, 1984; Elgar et al., 1994;
55 Davidson et al., 1996; Miles & Russell, 2004). Field and laboratory data (e.g. Dickson et al., 1995; Inch

56 et al., 2016) indicate that reflection is primarily proportional to the wave period and the effect of
57 wave height is negligible.

58 Muttray et al. (2006) indicate that reflection predictors based on ξ overestimate the effect of wave
59 breaking, and highlight the potential role of swash zone dynamics when predicting reflection. But,
60 while the description of reflection in terms of surf zone conditions has attracted a lot of attention,
61 literature describing wave energy reflection in terms of swash dynamics is rather limited. Guedes et
62 al (2011) observed no link between swash energy and ξ , implying that swash energy and wave
63 reflection are independent at the hourly scale. However, Martins et al. (2017) found a correlation
64 between peak swash potential energy and reflected wave energy at the time-scale of individual
65 waves on a steep, reflective, large-scale laboratory beach, suggesting that reflected waves energy can
66 be predicted based on detailed swash measurements.

67 Swash is far from a simple oscillation of the waterline. Whitham (1958) and Shen & Meyer (1963)
68 introduced a parabolic ballistic approach for run-up as a solution for a collapsing bore running over
69 a dry beach. Hughes et al. (1997), Guard & Baldock (2007) and Power et al. (2011) showed in the
70 field and with laboratory measurements that swash flow can be far from symmetric, with the
71 antagonistic effects of wave energy and gravity over beach slope. On the other hand, Guza & Bowen
72 (1976) depict the swash as the antinode of a standing wave for non-breaking waves, with a rather
73 symmetric runup shape. Observations show that runup asymmetry results predominantly from the
74 effect of bore dissipation during the uprush, which occurs mainly due to breaking and friction
75 (Hughes & Fowler, 1995; Puleo & Holland, 2001), and this includes the influence of sediment grain
76 size (Masselink & Hughes, 1998, Elfrink & Baldock, 2002) but also swash-swash interactions
77 (Baldock & Holmes, 1999; Hughes & Moseley, 2007); catch-up and absorption during the uprush, and
78 collision between uprush and the preceding backwash (Chen et al., 2016). Large values of runup
79 asymmetry are thought to indicate large dissipation and weak reflection. Because the measurement
80 of reflection and swash is a difficult task in the field, observations are scarce. Nonetheless, current
81 remote sensing techniques such as video imagery (Power et al., 2011; Almar et al., 2017) or LiDAR
82 (Blenkinsopp et al., 2010) are capable of obtaining suitable data.

83 This paper stresses the role played by swash in controlling reflection, which is ignored in most
84 common predictors based on surf zone conditions. A predictor for wave reflection based on swash
85 asymmetry is introduced and validated using datasets collected at three contrasting natural beaches
86 covering a range of conditions from dissipative to highly reflective. We investigate the advantage of
87 using swash dynamics for predicting reflection rather than the surf similarity parameter ξ , in

88 particular at complex beaches and hourly timescales. Finally, the role of asymmetry to indicate
89 “swash similarity” is discussed and some concluding remarks are provided.

90

91 2. Data and methods

92 Data were collected during three experiments undertaken in 2012-2013 at three different field
93 sites (Figure 1), ranging from dissipative to reflective beach slopes and low to high energetic wave
94 conditions. The corresponding hydro-morphological conditions during the three experiments are
95 shown in Figure 2.

96 A dissipative beach (upper beach slope $\alpha=0.05$) experiment was conducted at Mataquito, Chile,
97 from November 28th to December 14th, 2012 (Cienfuegos et al., 2014). Mataquito is a medium grain-
98 sized ($D_{50}=0.2$ mm), alongshore uniform, barred beach with a micro-tidal range and a wave climate
99 dominated by swell waves (annual mean derived from EraInterim -ECMWF, Dee et al., 2011- for the
100 1979-2012 period, $H_s \sim 2.4$ m, $T_p \sim 12$ s, SW). During the experiment, tidal amplitude ranged from
101 0.4 to 1 m. A large swell hit the coast on Dec. 2, ($H_s = 4$ m, $T_p = 18$ s, day 3 in Fig. 2, left panels), followed
102 by moderately energetic conditions starting on Dec. 5 ($H_s = 1-2$ m, $T_p = 10-15$ s).

103 An intermediate beach (upper beach slope $\alpha=0.12$) experiment was conducted at Nha Trang,
104 Vietnam, from December 3rd to 10th, 2013 (Lefebvre et al., 2014). Nha Trang is a uniform low-tide
105 terrace, medium grain-sized ($D_{50}=0.3$ mm) beach with a micro-tidal range and a low to moderate
106 energy wave climate (annual mean, $H_s < 1$ m, $T_p < 5$ s, E). During the experiment, tidal amplitude
107 decreased from 1.2 to 0.5 m. Wave height and period decreased continuously, from $H_s = 1$ m, $T_p = 9$ s
108 to $H_s = 0.5$ m and $T_p = 5$ s.

109 A reflective beach (upper beach slope $\alpha=0.15$) experiment was conducted at Grand Popo, Benin,
110 from February 17th to 28th, 2013. Grand Popo is a reflective, medium to coarse grain-sized ($D_{50}=0.6$
111 mm), alongshore uniform, low-tide terraced beach with a micro-tidal range and a wave climate
112 dominated by swell waves (annual mean, $H_s \sim 1.4$ m, $T_p \sim 9.4$ s, SW) (Almar et al., 2014a). During the
113 experiment, tidal amplitude increased from 0.5 m to 1.4 m. An energetic swell hit the coast on Feb.
114 23, ($H_s = 1.5$ m, $T_p = 18$ s), followed by moderate conditions.

115 At each site, the upper beach slope was extracted from daily topographic surveys undertaken at
116 low tide using differential GPS. Directional wave measurements were obtained in approximately 10
117 m water depth (red circles in Fig. 1) using an Acoustic Doppler Current Profiler (ADCP Workhorse
118 Sentinel 1200 KHz, 20-min wave bursts; see method in Jeans et al., 2002). Shore-based video swash
119 monitoring was undertaken at 2 Hz during daylight hours at the three experiment sites. Time series
120 of pixel intensity sampled along a cross-shore line (time stacks) (Holland & Holman, 1993) were

121 collected to measure wave runup, which was detected by applying a Radon Transform (RT) approach
 122 described in Almar et al. (2017). In this study, the ability of the RT to detect the instantaneous
 123 shoreline was assessed by comparison to concurrent LiDAR measurements and compared to the
 124 commonly used color contrast method (CC), which defines the waterline from RGB colorband
 125 contrast. Because the RT is based on motion detection it is more able than the CC approach for
 126 distinguishing between backwash and the groundwater seepage line, and is less sensitive to poor
 127 light conditions. Rectification of images from pixels into real-world coordinates was accomplished
 128 by direct linear transformation using DGPS ground control points (Holland et al., 1997) after a
 129 correction of the radial lens distortion (Heikkila & Silven, 1997). Although varying somewhat
 130 throughout the field of view, the pixel footprint was less than 0.1 m in the cross-shore direction over
 131 the region of interest (surf-swash zones). A single cross-shore transect was considered at the three
 132 sites, assuming alongshore-uniform processes, which will not be the case in the presence of
 133 longshore variability in the swash dynamics induced by irregular features such as crescentic sandbar
 134 (Nicolae Lerma et al., 2017) and beach cusps (Almar et al., 2018).

135 Swash energy flux F_{swash} was computed from 1-hr video time stacks (Power et al., 2011; Guedes et
 136 al., 2011; Senechal et al., 2011):

137

$$138 \quad F_{swash} = E_{swash} C_{gsw} \sim \frac{\rho g R_{sw}^2}{16} \quad (\text{Eq. 2})$$

139

140 Where ρ is water density (here 1025 kg/m³) and R is the horizontal runup computed from
 141 horizontal waterline timeseries S , $R_{sw} = 4(S \tan \alpha_{sw})$, using the RT (Radon Transform method, see
 142 Almar et al., 2017) and α_{sw} as the active swash slope, which is defined by Holland and Puleo (2001)
 143 as the dynamic slope within the swash zone which changes with tide. A constant shallow water group
 144 velocity is considered hereafter $C_{gsw} = \sqrt{gh} \sim 1 \text{ m/s}$, using an arbitrary depth of 0(10 cm) at swash
 145 inception, due to the lack of information. The directional wave spectra $E_d(\theta, f)$ were computed from
 146 an ADCP (Acoustic Doppler Current Profiler from RD Instrument), using the WavesMon software
 147 (see the manual) and the procedure described by Krogstad et al. (1988) and Strong et al.
 148 (2000). Incoming and reflected wave energy and direction were computed from co-localized pressure
 149 and current measurements from an ADCP (Acoustic Doppler Current Profiler, e.g. Sheremet et al.,
 150 2001). Though this technique is commonly used and offers good skill in retrieving swell band waves
 151 in intermediate to shallow depths (Herbers and Lentz, 2010), it can have some difficulty in capturing
 152 short wind waves due to the attenuation of the wave orbital motion with depth. Several methods
 153 exist to separate incoming and outgoing waves: the PUV temporal (e.g. Guza et al., 1974) and spectral

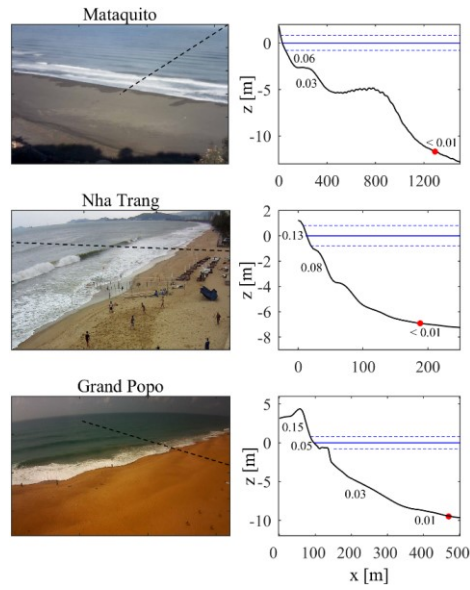
154 ~~(Sheremet et al., 2002) methods, using pressure and velocity sensors, and array methods that only~~
 155 ~~use cross-shore array of pressure sensors (or any free surface measurements), such as the recent~~
 156 ~~method based on the Radon Transform developed by Almar et al., (2014b). Here, ~~incoming~~ incoming~~
 157 ~~and outgoing wave heights were defined separated using from $E_d(\theta, f)$ the ADCP spectra following~~
 158 ~~the method described by Sheremet et al. (2002), integrating from the lower to upper cut-off~~
 159 ~~frequency (range set to gravity-infragravity band 0.02 Hz-0.5 Hz), ~~based on the local shore-normal~~~~
 160 ~~direction:~~

$$161 \quad H_{inc} = 4 \left(\int_{0.02 \text{ Hz}}^{0.5 \text{ Hz}} \int_{-90^\circ}^{90^\circ} E_d(\theta, f) d\theta df \right)^{1/2} \quad (\text{Eq. 3})$$

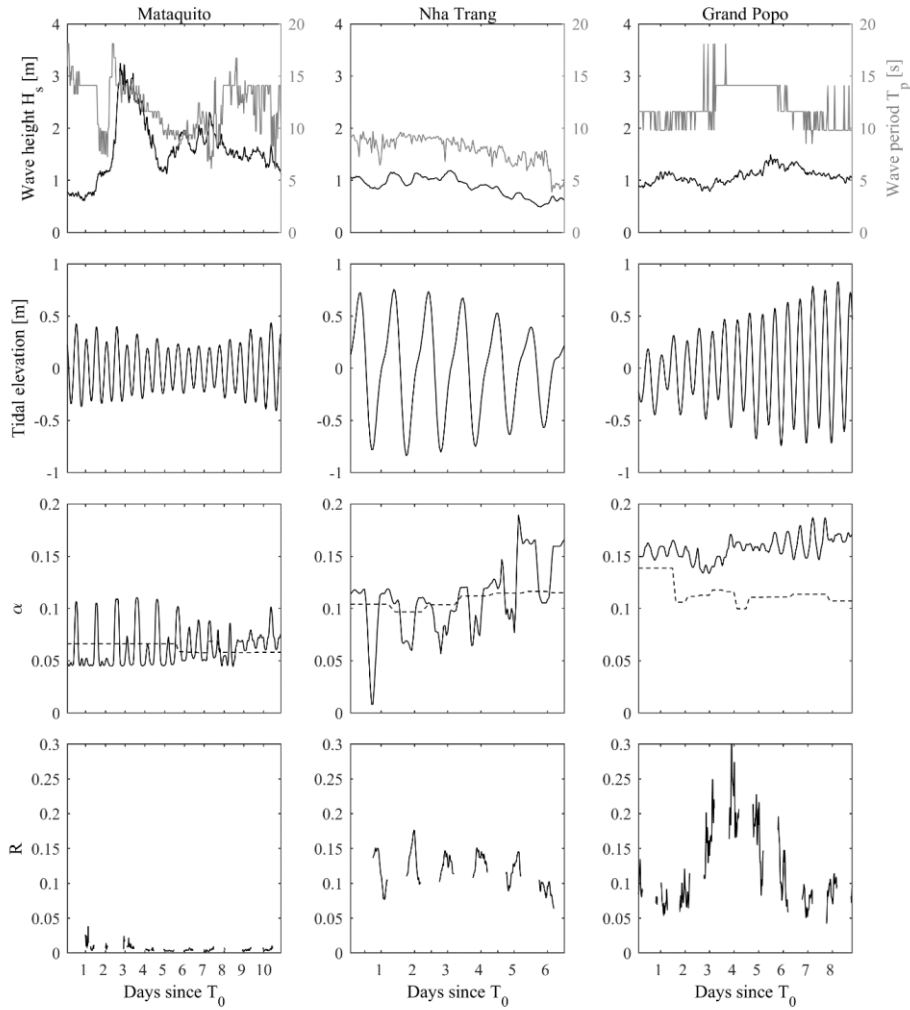
$$162 \quad H_{out} = 4 \left(\int_{0.02 \text{ Hz}}^{0.5 \text{ Hz}} \int_{270^\circ}^{90^\circ} E_d(\theta, f) d\theta df \right)^{1/2} \quad (\text{Eq. 4})$$

163 With $E_d(\theta, f)$ denoting the energy density and the term inside the parentheses representing the
 164 variance associated with the defined frequency band and the incidence angle from the shore-normal
 165 direction ~~(see also Almar et al., 2014b)~~. Peak period T_p is calculated as the inverse of the peak
 166 frequency in $E_d(\theta, f)$. Offshore incoming and reflected wave fluxes, F_{inc} and F_{ref} are computed as $F =$
 167 $ECg = \rho g H_s^2 T_p / 32\pi$ ($W.m^{-1}$) at the ADCP (depth~10m at the three sites), ~~Cg assuming being~~
 168 ~~computed with linear theory using intermediate depth conditions deep water conditions for~~
 169 ~~convenience, even if long waves might be slightly shoaling at ADCP locations during energetic~~
 170 ~~conditions~~. Reflection is quantified as the ratio of reflected and incoming energy. At all sites, the ADCP
 171 was moored sufficiently far offshore to avoid reflection coefficient variability associated with the surf
 172 zone, as described by Baquerizo et al. (1997).

173



174
 175 Figure 1: Snapshots from video systems (left) and (right) bathymetry profiles, (top) Mataquito,
 176 (mid) Nha Trang, and (bottom) Grand Popo. In the left panels, dashed black lines indicate the cross-
 177 shore time stack locations. In the right panels, numbers are local beach slopes, the red circles, solid
 178 and dashed blue lines indicate the location of the ADCP, mean sea level, max and min spring tidal
 179 elevations, respectively.



180
 181 Figure 2: From left to right, Mataquito, Nha Trang and Grand Popo experiments. (Row 1) offshore
 182 significant wave height (H_s - black line) peak period (T_p - grey line), (Row 2) tide, (Row 3) shoreface
 183 slope α with (active swash slope, solid line) or without (dashed line) tidal modulation. (Row 4)
 184 reflection (R).

185

186 3. Results

187 3.1. Nearshore wave energy budget

188 It is hypothesized that it is essential to account for swash processes when estimating R and the
189 nearshore energy balance, in particular at reflective or complex beaches. This is investigated here
190 through the decomposition of the nearshore wave energy budget (e.g. Baquerizo et al., 1998; Carini
191 et al., 2015). The nearshore wave energy budget (e.g. Sheremet et al., 2001) may be expressed as:

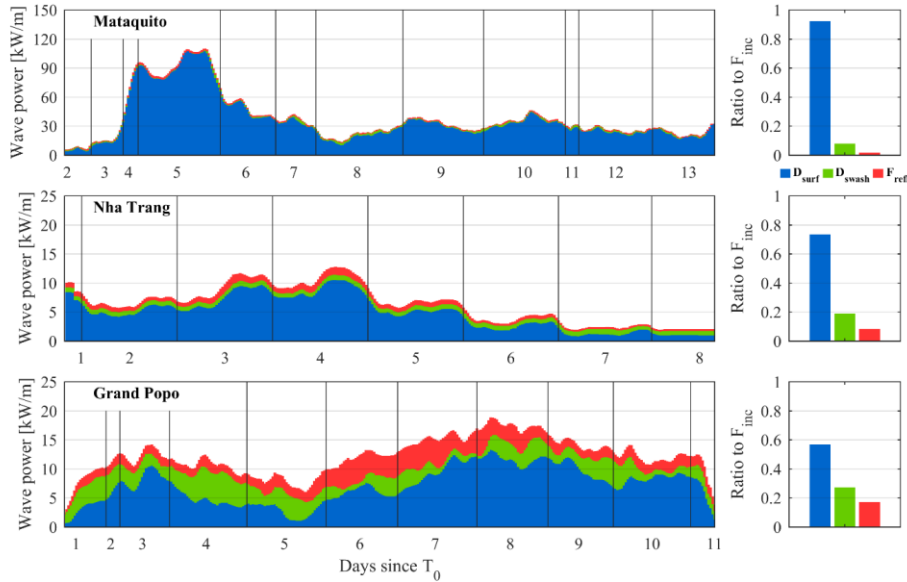
$$193 \quad F_{inc} - F_{ref} = D_{surf} + D_{swash} \quad (\text{Eq. 5})$$

194
195 With F_{inc} and F_{ref} the offshore incoming and reflected wave fluxes, D_{surf} and D_{swash} the wave
196 dissipation in the surf and swash zone respectively. We assume hereafter that reflection occurs only
197 in the swash zone, with the reflection from submerged bars considered to be negligible (for now) and
198 incident waves sufficiently shore-normal to be reflected back offshore and not get trapped (only
199 leaky modes). Swash energy flux F_{swash} computed in Eq. 2 can also be considered as:

$$201 \quad F_{swash} = D_{swash} + F_{ref} \quad (\text{Eq. 6})$$

202
203 Eq. 6 can only be satisfied under the assumption that reflected waves do not break when
204 propagating offshore and hence no energy is lost. Figure 3 shows the hourly evolution of D_{swash} , F_{ref}
205 and D_{surf} . F_{inc} and F_{ref} are measured at the ADCP (see Data and Methods Section) and D_{swash} is computed
206 from Eq. 6, D_{surf} is computed from the combination of Eq. 5 and 6. Figure 3 shows that the relative
207 contribution of D_{swash} increases with beach gradient. It is as small as 2 % at Mataquito, increases to
208 23 % at Nha Trang and up to 35 % at Grand Popo with the reflection coefficient R increasing in a
209 similar manner with values of 1%, 10% and 15 % respectively. As observed by Elgar et al. (1994) and
210 Miles and Russell (2001) R values are generally higher during high tide which is consistent with
211 higher reflection from a steeper beach face. At the two most reflective beaches, Grand Popo and Nha
212 Trang, the dissipation in the swash zone is important, due to the limited wave breaking over the
213 narrow terrace, in particular at high tide as also observed by Miles & Russell, (2004). Under such
214 conditions, swash plays a major role in governing the amount of reflected energy, as shown recently
215 by Martins et al., (2017). In contrast, dissipative beaches such as Mataquito are dominated by
216 breaking processes (Guedes et al., 2011), with minimal influence from the tide level.

217
218



219
 221 Figure 3: Left panels show a decomposition of the incoming wave power F_{inc} separated into surf
 222 zone dissipation D_{surf} (blue) from the combination of Eq. 5 and 6, swash zone dissipation D_{swash} (green)
 223 from Eq. 6, and reflected wave energy flux F_{ref} (red). The percentage contribution of each component
 224 to the total energy flux is shown in the right panels.

225
 226 *3.2. Wave reflection from runoff asymmetry*

227 Reflection measurements typically require the installation of instrumentation in intermediate
 228 water depths. The ability to estimate reflection based on swash characteristics would be beneficial
 229 and makes in-situ instrumentation redundant. We hypothesize here that D_{swash} is proportional to
 230 F_{swash} with $D_{swash} = K F_{swash}$ where K is an empirical coefficient that represents swash dissipation:

231
 232
$$K = (F_{swash} - F_{ref})/F_{swash} \quad (\text{Eq. 7})$$

233
 234 Laboratory measurements in the swash zone supported by numerical modelling such as in
 235 ~~Martins et al. (2017) estimate the bulk of energy reflected from the beach. A 0.5 coefficient of~~
 236 proportionality was found between reflected bulk and swash energy.

237

238 In accordance with the notion of surf similarity, a long wave on a mild slope would represent
239 comparable hydrodynamic conditions as a short wave and a steeper slope (Battjes, 1974). In other
240 words, a given swash slope appears steeper to longer waves than it does to shorter waves. As
241 observed for runup on rubble mound by several authors (e.g. Davidson et al., 1996), on a steeper
242 slope, more energy will be reflected (i.e. less energy will be dissipated). By contrast, a short wave on
243 a flat beach will dissipate its energy through bore breaking-induced turbulence and bottom friction
244 in the uprush which results in a thin layer of weak return flow during the backwash phase of the
245 swash cycle.

246 Figure 4 illustrates the contrasting swash shapes observed at the three sites. At Mataquito, the
247 runup time series presents a sawtooth shape; the already broken bore (Guard and Baldock, 2004) in
248 combination with a gentle swash slope leads to almost complete energy dissipation during the
249 uprush with a weak backwash. In contrast, at more reflective beaches, such as Nha Trang and even
250 more so at Grand Popo, large bores collapse at the shoreline and the steeper slope leads to strong
251 backwash which seemingly generates significant reflected wave energy (Martins et al., 2017). The
252 variability in uprush/backwash flows discussed above is characterized here through the front-to-lee
253 (temporal) asymmetry (see Elgar and Guza, 1985):

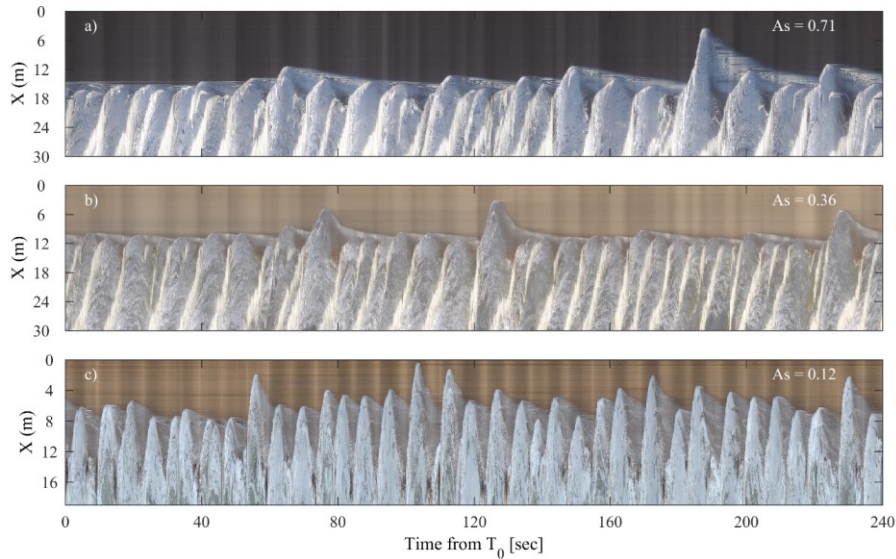
254

$$255 \quad A_s = \frac{\langle H^3(S-\bar{S}) \rangle}{\langle (S-\bar{S})^2 \rangle^{3/2}} \quad (\text{Eq. 8})$$

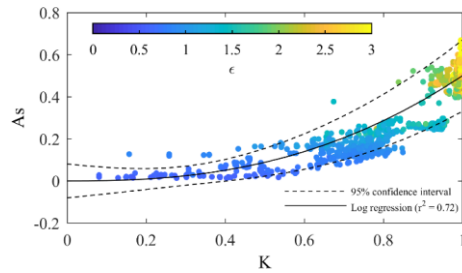
256

257 Where H denotes the Hilbert transform and S represents the horizontal swash excursion, $\langle \rangle$
258 indicates time averaging. Figure 4 shows an illustration of different swash conditions with the
259 corresponding runup asymmetry values ranging from pitched forward, dominated by uprush
260 ($A_s=0.71$) at Mataquito, to almost symmetrical ($A_s=0.12$) at Grand Popo.

261



262
 263 Figure 4: Illustration of video time stacks of the swash zone with asymmetry values at dissipative
 264 Mataquito (top), intermediate Nha Trang (mid) and reflective Grand Popo beaches (bottom).
 265



266
 267 Figure 5: Hourly runup asymmetry As (Eq. 8) (computed from the three datasets) as a
 268 function of the swash dissipation parameter K (Eq. 7). Colours represent the Miche swash similarity
 269 parameter ϵ ($\epsilon = S \frac{\omega^2}{g} \alpha_{sw}$, where S is the horizontal swash excursion, α_{sw} is the active swash slope, g
 270 is the acceleration due to gravity and ω is the angular wave frequency $2\pi/T$ with the swash period
 271 T). The solid line is a logarithmic regression and dashed lines show the 95% confidence intervals.
 272

273 In Figure 5, the aggregate of all of the data collected from the three sites is presented in terms of
 274 the swash reflection parameter, the corresponding swash similarity parameter (colour) and the

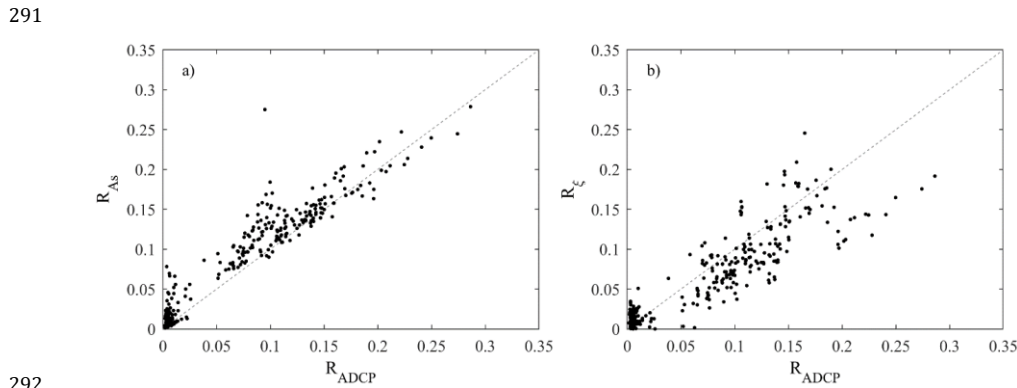
275 estimated asymmetry. It can be noted that there is a positive correlation between swash asymmetry
 276 and swash dissipation. A functional form can be obtained as:

$$277 \quad K = aAs^b \quad (\text{Eq. 9})$$

279 Where logarithmic best fit regression gives $a=1.3$ and $b=0.4$ (significant at 95% level, Figure 5). It
 280 is now possible to estimate the reflection coefficient directly as a function of the remotely sensed
 281 swash asymmetry:

$$282 \quad R_{As} = \frac{F_{swash}(1-K)}{F_{inc}} \quad (\text{Eq. 10})$$

283
 284
 285
 286 Figure 6 indicates a strong relationship between hourly R_{As} and reflection observed offshore R_{adcp} ,
 287 with a coefficient of determination of 0.72 (significant at 95% level). Method skill worsens for low
 288 reflection values as the Mataquito data is clustered with no clear dependence on As (see Figure 5).
 289 However, this swash-based predictor offers a better result for these three datasets than conventional
 290 predictor based on surf conditions (following the surf similarity parameter $R_\xi = 0.1\xi^2$, with $R^2 = 0.38$).



292
 293 Figure 6: Predicted hourly reflection coefficients from a) runup asymmetry R_{As} and b)
 294 conventional predictor based on surf conditions using Battjes's formula $R_\xi=0.1\xi^2$, as a function of
 295 observed reflection coefficient from ADCP R_{adcp} . Dashed lines show 1:1 agreement.

296

297 **4. Discussion**

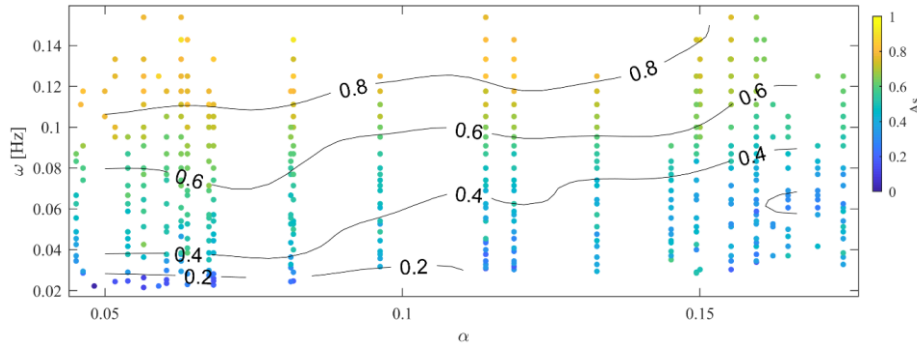
298 Runup asymmetry is an all-encompassing parameter that is the result of surf and swash zone
299 wave transformation, and their interaction with morphology. The strongest agreement between
300 asymmetry and wave reflection is found at the most reflective Grand Popo and Nha Trang beaches.
301 This relationship weakens at the dissipative Mataquito beach, where the dependence of reflection on
302 swash dynamics also weakens (see the surf scaling parameter, Guza and Inman, 1975). In such a case,
303 the reflection can be scaled more appropriately using deep-water parameters (Guza & Thornton,
304 1982; Diaz-Sanchez et al., 2013). The results show that a swash-based reflection proxy is less
305 accurate at dissipative beaches, where runup asymmetry may not be the key controlling factor, or
306 the noise in the reflection data is large compared to the signal itself. This is in line with the
307 observation of Guedes et al., (2011). While the newly developed runup asymmetry predictor is
308 clearly advantageous in comparison with other predictors at two-slope beaches (i.e. different swash
309 and surf slopes) it might be affected by the presence of a submerged sandbar such as observed at
310 Mataquito. Irregular morphological features, such as sandbars, can also introduce multiple reflecting
311 and energy dissipating features (Davies, 1982; Mei, 1985; Bailard et al., 1992; Elgar et al., 2003; Almar
312 et al., 2018) which inherently weakens the link between swash dynamics and offshore waves. Waves
313 transmitted over the bars may undergo partial reflection at the shoreline (Miche, 1951; Elgar et al.,
314 1994), followed by re-reflections from the bars, complicating the wave transformation (Yu and Mei,
315 2000). Noteworthy, the scatter observed in Figure 6 can be partly attributed to the noise in F_{ref} and
316 F_{inc} estimated at the ADCP. As described in Section 2 (Data and methods), the ADCP can have
317 difficulties to retrieve waves at the lower and upper cut-off frequencies, in particular in capturing
318 short wind waves (e.g. Nha Trang) in relatively deep water and longest waves (e.g. Mataquito).

319 Identifying the backwash leading edge is notoriously difficult from video imaging and much can
320 be left up to interpretation as the leading edge infiltrates into the bed (Vousdoukas, 2014). The RT
321 method (Almar et al., 2017) is based on motion (i.e. flow) detection rather than colour contrast used
322 in pioneering studies of Holland & Holman (1993) and Holland et al. (1995, 2001). Whereas no
323 substantial differences are expected in terms of swash statistics, the RT might be more suited when
324 studying swash shape, such as asymmetry, as it describes main flow behaviour rather than the
325 behaviour of a weak backwash flow. Most swash models, for example, the ballistic approach of Shen
326 et Meyer (1963) do not account for swash asymmetry and the influence of swash interactions
327 (Bergsma et al., 2018) on the characteristics of the shoreline motion. This is because these sources of
328 energy loss predominately occur seaward of the instantaneous shoreline through the interaction of
329 the incoming bore with the preceding backwash (Baldock and Holmes, 1999). Our data shows that

330 runup shape, which reflects the level of dissipation, can vary substantially; part of this observed
331 variability could be attributed to the dissipation resulting from these swash interactions (Baldock &
332 Holmes, 1999; Hughes & Mosseley, 2007; Brocchini and Baldock, 2008). While the long period swell
333 waves and steep beach at Grand Popo were observed to lead to minimal interactions, interactions
334 were common at Mataquito. The long-duration return flow of short waves over flat beaches has the
335 potential to enhance swash-swash interaction, dissipating energy and promoting an asymmetric
336 shape.

337 The normalized swash slope parameter (Battjes et al., 2004) suggests that swash dynamics is
338 primarily influenced by wave period and active swash slope, and thus potentially runup asymmetry
339 A_s . Following the approach in Martins et al., (2017), the range of A_s values for different swash slopes
340 and periods is investigated on an individual swash basis. In Figure 7, the distribution of A_s averaged
341 over the three experiments is presented as a function of swash slope α and swash frequency ω . A_s
342 decreases with α and increases with ω : for a given slope, shorter swashes tend to have higher
343 dissipation (strong A_s) while longer swashes reflect more energy (weak A_s). In a similar manner to
344 the estimation of reflection from the combination of A_s and runup excursion length, this suggests that
345 A_s and ω could be used to estimate swash slope remotely. Because swash hydrodynamics adapt more
346 rapidly than morphology to rapidly varying offshore conditions, there is the potential for high-
347 frequency A_s and subsequent reflection to provide a short-term predictor of beach slope evolution,
348 though further analysis is required to confirm this.

349 This new reflection predictor based uniquely on swash dynamics offers the potential to estimate
350 reflection using shore-based remote sensing systems such as video cameras. These tools enable
351 inexpensive and relatively simple long-term monitoring of swash motion (e.g. Guedes et al., 2011;
352 Almar et al, 2017) and hence reflection (via the new predictor), and this has significant advantages
353 over more conventional reflection measurement approaches which require costly in-situ marine
354 deployments and are typically limited to relatively short durations (e.g. Baquerizo et al., 1997). In the
355 current work, only a single cross-shore transect was analysed, however two-dimensional
356 information on reflection can be obtained by extracting swash motion and A_s at several alongshore
357 locations which may give new insight into the longshore variability of wave reflection and its effect
358 on surf zone dynamics (Nicolae Lerma et al., 2017; Almar et al., 2018).



359
 360 Figure 7: Distribution of runup asymmetry A_s as a function of swash frequency ω (inverse of
 361 individual swash duration) and active swash slope α . Dashed black contour lines represent iso-
 362 asymmetry levels.

363

364 5. Conclusions

365 A new predictor for wave reflection using video-derived runup asymmetry is proposed and
 366 applied to dissipative, intermediate and reflective beaches. A decomposition of the incoming wave
 367 energy fluxes into surf and swash zone dissipation and reflected waves showed that it is essential to
 368 account for swash-zone processes when estimating reflection, in particular at intermediate and
 369 reflective beaches. Our results show that runup asymmetry in uprush/backwash is correlated with
 370 swash dissipation: strong values of runup asymmetry indicate large swash-based energy dissipation.
 371 For our dataset, the new predictor based on remotely-sensed swash characteristics offers improved
 372 results ($R^2=0.72$) with better skill in comparison to conventional predictors based on surf similarity
 373 ($R^2=0.38$). This is because runup is the result of surf and swash zone wave transformation, and their
 374 interaction with the local morphology. In addition, it is shown that runup asymmetry reflects an
 375 equilibrium between swash period, slope and dissipation.

376

377 Acknowledgments

378 Mataquito exp. supported by Chilean CONICYT grants FONDECYT/1120878 and
 379 FONDAP/15110017, Grand Popo exp. by French INSU/CNRS EC2CO-LEFE/IRD, UNESCO co-chair
 380 ICPMA/IRHOB, and Nha Trang exp. by Vietnamese MOST (BKHCN/NDT-HD/2013/110) and MOST2:
 381 NDT.24.FRA/16. We are greatly indebted to the naval services of Benin at Grand Popo for their
 382 logistic support during the field experiment and for allowing the installation of the permanent video
 383 system on the semaphore. This research has received support from French grants through ANR

384 (COASTVAR: ANR-14-ASTR-0019). PAC also received support through CONICYT grants
385 FONDECYT/1107415 and PIA/Basal FB0821.

386

387 **References**

388 Abdelrahman, S.M., Thornton, E.B., 1987. Changes in the short wave amplitude and wavenumber due
389 to the presence of infragravity waves. Proceedings of the Specialty Conference on Coastal
390 Hydraulics. American Society of Civil Engineers, New York, 458-478

391 Ahrens, J.P., 1979. Irregular wave runup, Coastal Struct.'79, Am. Soc. of Civ. Eng., New York, 998-1019

392 Almar, R., Cienfuegos, R., Gonzalez, E., Catalan, P.A., Michallet, H., Bonneton, P., Castelle, B., Suarez, L.,
393 2012. Barred-beach morphological control on infragravity motion, International Conference on
394 Coastal Engineering, Santander, Spain, 2-6 July 2012

395 Almar, R., Du Penhoat, Y., Honkonnou, N., Castelle, B., Laibi, R., Anthony, E., Senechal N., Degbe, G.,
396 Chuchla, R., Sohou, Z., Dorel, M., 2014a. The Grand Popo experiment, Benin, Journal of Coastal
397 Research, 70, 651-656, ISSN 0749-0208

398 [Almar, R., Michallet, H., Cienfuegos, R., Bonneton, P., Tissier, M.F.S., Ruessink, B.G., 2014b. On the use
399 of the radon transform in studying nearshore wave dynamics. Coast.
400 Eng. 92, 24-30](#)

401 Almar, R., Almeida, P., Blenkinsopp, C., and Catalan, P., 2016. Surf-swash interactions on a low-tide
402 terraced beach. Proceedings of the 14th International Coastal Symposium (Sydney, Australia).
403 Journal of Coastal Research, Special Issue, 75, 348-352

404 Almar, R., Blenkinsopp, C., Almeida, L.P., Cienfuegos, R., Catalan, P., 2017. Wave runup video detection
405 using the Radon Transform, Coastal Engineering, 130, 46-51

406 Almar, R., Nicolae Lerma, A., Castelle, B., Scott, T., 2018. On the influence of reflection over a rhythmic
407 swash zone on surf zone dynamics. Ocean Dynamics, 68(7), 899-909

408 Bailard J.A., Devries, J.W., Kirby, J.T., 1992. Considerations in using Bragg reflection for storm erosion
409 protection. Journal of Waterway, Port, Coastal and Ocean Engineering, 118, 62-86

410 Baldock, T.E., Holmes, P., 1999. Simulation and prediction of swash oscillations on a steep beach.
411 Coast. Eng. 36, 219-242

412 Baquerizo, A., Losada, M.A., Smith, J.M. Kobayashi, N., 1997. Cross-shore variation of wave reflection
413 from beaches J. Waterw. Port. Coast. Ocean Eng., 123, 274-279

414 Battjes, J., 1974. Surf similarity. 14th Coastal Engineering Conference, Am. Soc. Of Civ. Eng.,
415 Copenhagen, Denmark, 466-480

416 Battjes, J.A., Bakkenes, H.J., Janssen, T.T., van Dongeren, A.R., 2004. Shoaling of subharmonic gravity
417 waves, *J. Geophys. Res.*, 109, C02009, doi:10.1029/2003JC001863

418 Bergsma, E.W.J., Blenkinsopp, C.E., Martins, K., Almar, R. and Almeida, L.P., 2018. Observations and
419 automated detection of bore-collapse using LiDAR measurements at Nha Trang beach, Vietnam.
420 In revision for *Continental Shelf Research*

421 Blenkinsopp, C., Mole, M.E., Turner, I.L., Peirson, W.L., 2010. Measurements of the time-varying
422 profile across the swash zone using an industrial LIDAR, *Coastal Eng.*, 57, 1059-1065

423 Brocchini, M., Baldock, T.E., 2008. Recent advances in modeling swash zone dynamics: influence of
424 surf-swash interaction on nearshore hydrodynamics and morphodynamics, *Rev. Geophys.*, 46,
425 p. RG3003

426 Carini, R.J., Chickadel, C.C, Jessup, A.T., Thomson, J., 2015. Estimating wave energy dissipation in the
427 surf zone using thermal infrared imagery. *J. Geophys. Res. Oceans*, 120(6), 3937-3957,
428 10.1002/2014JC010561

429 Chen, X., Hofland, B., Uijttewaai, W., 2016. Maximum overtopping forces on a dikemounted wall with
430 a shallow foreshore. *Coastal Engineering* 116, 89-102

431 Cienfuegos, R., Villagran, M., Aguilera, J.-C., Catalan, P., Castelle, B., Almar, R., 2014. Video monitoring
432 and field measurements of a rapidly evolving coastal system: the river mouth and sand spit of
433 the Mataquito river in Chile. *Journal of Coastal Research*, SI 70, 639-644

434 Davies, A.G., 1982. The reflection of water-wave energy by undulations on the seabed, *Dynamics of*
435 *Atmos. and Oceans*, 6, 207-232

436 Davidson, M.A., Bird, P.A.D., Bullock, G.N., Huntley, D.A., 1996. A New Dimensional Number for the
437 Analysis of Wave Reflection from Rubble Mound Breakwaters, *Coastal Engineering* 29, 93-120

438 Dee, D.P. et al., 2011. The ERA-Interim reanalysis: configuration and performance of the data
439 assimilation system, *Q. J. R. Meteorol. Soc.*, 137, 553-597, doi:10.1002/qj.828.

440 Diaz-Sanchez, R., Lopez-Gutierrez, J., Lechuga, A., Negro, V., Esteban, M., 2013. Direct estimation wave
441 setup as a medium level in swash. *Proceedings 12th International Coastal Symposium*
442 *(Plymouth, England)*, *Journal of Coastal Research*, Special Issue, SI 65, 201-206

443 Dickson, W., Herbers, T.H.C., Thornton, E., 1995. Wave reflection from breakwater, *J. of Water., Port,*
444 *Coast., Ocean Eng.*, 121, 262-268

445 Elgar, S., Herbers, T., Guza, R., 1994. Reflection of ocean surface gravity waves from a natural beach.
446 *J. Physical. Oceanogr.*, 24(7), 1503-1511

447 Elgar, S, Guza RT. 1985. Observations of Bispectra of Shoaling Surface Gravity-Waves. *Journal of*
448 *Fluid Mechanics*, 161:425-448

449 Elgar, S., Raubenheimer, B., Herbers, T.H.C., 2003. Bragg reflection of ocean waves from sandbars,
450 Geophys. Res. Lett.30, 1016, 10.1029/2002GL016351

451 Elfrink, B., & Baldock, T., 2002. Hydrodynamics and sediment transport in the swash zone: a review
452 and perspectives. Coast. Eng., 45, 149-167.

453 Guard, P.A., Baldock, T.E., 2007. The influence of seaward boundary conditions on swash zone
454 hydrodynamics. Coastal Eng., 54(4), 321-331

455 Guedes, R., Bryan, K., Coco, G., Holman, R., 2011. The effects of tides on swash statistics on an
456 intermediate beach. Journal of Geophysical Research, 116, C04008

457 [Guza, R.T., and Davis, R.E., 1974. Excitation of edge waves by waves incident on a beach. J. Geophys.](#)
458 [Res. 79, 1285-1291](#)

459 Guza, R.T., Bowen, A.J., 1976 Finite amplitude edge waves. J. Mar. Res. 34, 269-293

460 Guza, R., Thornton, E., 1982. Swash oscillations on a natural beach. J. Geophys. Res., 87, 483-491

461 Hancock, M.J., Landry, B.J., Mei, C.C., 2008. Sandbar formation under surface waves: Theory and
462 experiments. Journal of Geophysical Research, 113, C07022

463 Heikkila, J., Silven, O., 1997. A four-step camera calibration procedure with implicit image correction.
464 Computer Vision and Pattern Recognition. In Proceedings of the IEEE Computer Society
465 Conference, 1106-11012

466 Herbers, T.H.C., Lentz, S.J., 2010. Observing directional properties of ocean swell with an Acoustic
467 Doppler Current Profiler (ADCP). Journal of Atmospheric and Oceanic Technology, 27, 210-225.

468 Holland, K.T. and Puleo, J., 2001. Variable swash motions associated with foreshore profile change,
469 Journal of Geophysical Research, 106, C3, 4613-4623

470 Holland, K.T., Holman, R.A., 1993, The statistical distribution of swash maxima on natural beaches, J.
471 Geophys. Res. , 87, 10, 271-10, 278

472 Holland, K., Holman, R., Lippmann, T., Stanley, J., Plant, N., 1997. Practical use of video imagery in
473 nearshore oceanographic field studies. Oceanic Engineering, 22(1), 81-82

474 Holland, K.T., Holman, R.A. 1993. The statistical distribution of swash maxima on natural beaches. J.
475 Geophys. Res., 98(C6), 10271-10278

476 Holland, K.T., Raubenheimer, B., Guza, R.T., Holman, R.A., 1995. Runup kinematics on a natural beach,
477 J. Geophys. Res., 100, 4985-4993

478 Holman, R.A., 1986. Extreme value statistics for wave run-up on a natural beach, Coastal Engineering,
479 9 (6), 527-544

480 Holman, R.A., Sallenger, A., 1985. Setup and swash on a natural beach. J. Geophys. Res., 90, 945- 953

481 Hughes, S., Fowler, J., 1995. Estimating wave-induced kinematics at sloping structures. *Journal of*
482 *Waterway, Port, Coastal, and Ocean Engineering*, 121(4), 209–215

483 Hughes, M.G., Masselink, G., Brander, R.W., 1997. Flow velocity and sediment transport in the swash
484 zone of a steep beach, *Marine Geology*, 138, 91-103

485 Hughes, S., Mosseley, A. 2007. Hydrokinematic regions within the swash zone. *Cont. Shelf Res.*,
486 27(15), 2000–2013

487 Inch, K., Davidson, M., Masselink, G., Russell, P., 2017. Observations of nearshore infragravity wave
488 dynamics under high energy swell and wind-wave conditions, In *Continental Shelf Research*,
489 138, 2017, 19-31, ISSN 0278-4343

490 Iribarren, C., Nogales, C., 1949. Protection des ports. XVIIth International Navigation Congress,
491 Section II, Communication, 31–80

492 Laibi, R., Anthony, E., Almar, R., Castelle, B., Senechal, N., 2014. Morphodynamic characterisation of
493 the human-impacted Bight of Benin sand barrier coast, West Africa, *Journal of Coastal Research*,
494 SI 70, 079-083, ISSN 0749-0208

495 Lefebvre, J-P., Almar, R., Viet, N., Uu, D., Thuan, D., Binh, L., Ibaceta, R., Duc, N., 2014. Contribution of
496 swash processes generated by low energy wind waves in the recovery of a beach impacted by
497 extreme events: Nha Trang, Vietnam. *Journal of Coastal Research*, SI 70, 663–668

498 Jeans, G., Primrose, C., Descusse, N., Strong, B., and van Weert, P., 2002. A Comparison between
499 Directional Wave Measurements from the RDI Workhorse with Waves and the Datawell
500 Directional Waverider, IEEE Seventh working Conference on Current Measurement Technology.

501 [Krogstad, H.E., Gordon, R.L. and Miller, M.C., 1988. High-resolution directional wave spectra from](#)
502 [horizontally-mounted acoustic Doppler current meters. *J. Atmos. and Oceanic Technol.*, 5, 340-](#)
503 [352](#)

504

505 Martins, K., Blenkinsopp, C.E., Almar, R., Zang, J., 2017. The influence of swash-based reflection on
506 surf zone hydrodynamics: a wave-by-wave approach. *Coastal Engineering*, 122, 27-43

507 Masselink, G., & Hughes, M., 1998. Field investigation of sediment transport in the swash zone. *Cont.*
508 *Shelf Res.*, 18, 1179-1199.

509 Mei, C.C., 1985. Resonant reflection of surface waves by periodic sand bars. *J. Fluid Mech.*, 152, 315-
510 335

511 Miche, R., 1951. Le pouvoir reflechissant des ouvrages maritimes exposes à l'action de la houle. *Ann.*
512 *Ponts Chaussees*, 121, 285–319

513 Miles, J., Russell, P., 2004. Dynamics of a reflective beach with a low tide terrace. *Continental Shelf*
514 *Research COAST3D Special Issue*, 24, 1219–1247

515 Mizuguchi, M., 1984. Swash on a natural beach. *Coastal Engineering Proceedings*, 19, 2156–1028.

516 Muttray, M., Oumeraci, H., Ten Oever, E., 2006. Wave reflection and wave run-up at rubble mound
517 breakwaters, *Proc. of ICCE, San Diego, California*

518 Nicolae Lerma, A., Pedreros, R., Robinet, A., Sénéchal, N., 2017. Simulating wave setup and runup
519 during storm conditions on a complex barred beach. *Coastal Engineering*, 123, 29-41

520 O'Hare, T.J., Davies, A.G., 1993. Sand bar evolution beneath partially-standing waves: Laboratory
521 experiments and model simulations, *Cont. Shelf Res.*, 13, 1149-1182

522 Power, H., Holman, R., Baldock, T., 2011. Swash zone boundary conditions derived from optical
523 remote sensing of swash zone flow patterns. *J. of Geophysical Research*, 116, 06007.

524 Puleo, J.A., Holland, K.T., 2001. Estimating swash zone friction coefficients on a sandy beach. *Coastal*
525 *Eng.*, 43(1), 25–40

526 Raubenheimer, B., Guza, R.T., Elgar, S., Kobayashi, N., 1995. Swash on a gently sloping beach, *J.*
527 *Geophys. Res.*,100(C5), 8751–8760, doi:10.1029/95JC00232

528 Raubenheimer, B., Guza, R.T., Elgar, S., 1996. Wave transformation across the inner surf zone,*J.*
529 *Geophys. Res.*,101, 25, 589–25, 597,doi:10.1029/96JC02433

530 Rocha, M., Michallet, H., Silva, P., 2017. Improving the parameterization of wave nonlinearities—The
531 importance of wave steepness, spectral bandwidth and beach slope, *Coastal Eng.*, 121, 77–89.

532 Ruessink, B.G., Kleinhans, M.G., van den Beukel, P.G.L., 1998. Observations of swash under highly
533 dissipative conditions, *J. Geophys.Res.*,103(C2), 3111–3118, doi:10.1029/97JC02791

534 Ruggiero, P., Komar, P.D., McDouglas, W.G., Marra, J.J., Beach, R.A., 2001. Wave runup, extreme water
535 levels and erosion of properties backing beaches. *Journal of Coastal Research*, 17 (2),407-419

536 Seelig, W.N., Ahrens, J.P., 1981. Estimation of wave reflection and energy dissipation coefficients for
537 beaches, revetments and breakwaters. CERC Technical paper 81-1, Fort Belvoir, U.S.A.C.E.,
538 Vicksburg, MS

539 Senechal, N., Coco, G., Bryan, K.R. Holman, R.A., 2011. Wave runup during extreme storm conditions,
540 *J. Geophys. Res.*, 116 (7), p. C07032

541 Shen, M.C., Meyer, R.E., 1963. Climb of a bore on a beach part 3. run-up. *J. Fluid Mech.*, 16, 113125.

542 [Krogstad, H.E., Gordon, R.L. and Miller, M.C., 1988. High-resolution directional wave spectra from](#)
543 [horizontally-mounted acoustic Doppler current meters. *J. Atmos. and Oceanic Technol.*, 5, 340-](#)
544 [352](#)

545 [Sheremet, A., Guza, R.T., Elgar, S., Herbers, T.H.C., 2002. Observations of nearshore infragravity](#)
546 [waves: seaward and shoreward propagating components. J. Geophys. Res. 107,](#)
547 <http://dx.doi.org/10.1029/2001JC000970.C8>

548 ~~Sheremet, A., R. Guza, S. Elgar, Herbers, T., 2001. Estimating infragravity wave properties from~~
549 ~~pressure-current meter array observations, paper presented at 27th International Conference~~
550 ~~on Coastal Engineering, Am. Soc. of Civ. Eng., Sydney, Australia~~

551 [Strong, B., Brumley, B., Terray, E.A., Stone, G.W., 2000. The performance of ADCP-derived directional](#)
552 [wave spectra and comparison with other independent measurements. OCEANS 2000 MTS/IEEE](#)
553 [Conference and Exhibition. Conference Proceedings. DOI: 10.1109/OCEANS.2000.881763](#)

554 Sutherland, J., O'Donoghue, T., 1998. Characteristics of wave reflection spectra. J. Waterw. Port
555 Coastal Ocean Eng., 124(6), 303-311

556 Tatavarti, R.V., Hunfley, D.A., and Bowen, A.J., 1988. Incoming and outgoing wave interactions on
557 beaches, Proceedings of the 21 Coastal Engineering Conference, American Society of Civil
558 Engineers, 1, 136-150

559 Vousdoukas, M.I., 2014. Observations of wave run-up and groundwater seepage line motions on a
560 reflective-to-intermediate, meso-tidal beach. Marine Geology 350. DOI:
561 10.1016/j.margeo.2014.02.005

562 Whitham, G.B., 1958. On the propagation of shock waves through regions of non-uniform area of flow.
563 J. of Fluid Mechanics 4, 520-539

564 Yu, J., Mei, C.C., 2000. Formation of sand bars under surface waves. J. Fluid Mech. 416, 315-348

Formatted: French (France)